Convective heat transfer in ribbed square channels

C. Nonino and G. Comini
Università degli Studi di Udine, Dipartimento di Energetica e Macchine, Udine, Italy

Received November 2001
Accepted March 2002

Keywords *Heat transfer, Flow, Friction, Finite elements*

Abstract *Three-dimensional laminar forced convective heat transfer in ribbed square channels is investigated. In these channels, transverse and angled ribs are placed on one or two of the walls to form a repetitive geometry. After a short distance from the entrance, also the flow and the dimensionless thermal fields repeat themselves from module to module allowing the assumption of periodic, or anti-periodic, conditions at the inlet/outlet sections of the calculation cell. Prescribed temperature boundary conditions are assumed at all solid walls, including the ribs. Pressure drop and heat transfer characteristics are compared for rib angles ranging from 90° (transverse ribs) to 45°, and different values of the Reynolds number. The influence of rib geometries is investigated below and above the onset of the self-sustained flow oscillations that precede the transition to turbulence. Numerical simulations are carried out employing an equal order finite-element procedure based on a projection algorithm.*

Nomenclature

a = independent variable
A = amplitude
f = friction factor
h = average convection coefficient
H = height of the channel
k = thermal conductivity
L = length
$\dot{m}$ = mass flow rate
n = outward oriented normal to the external surface
Nu = overall Nusselt number
p = pressure
$\tilde{p}$ = periodic component of pressure
q = heat flow rate
Pr = Prandtl number
Re = Reynolds number
S = surface
St = Strouhal number
t = temperature
T = dimensionless temperature
u,v,w = velocity components in the (x,y,z) directions
v = velocity vector
W = width of the channel
x,y,z = Cartesian coordinates
α = overall pressure gradient in the flow direction

Greek

ε = goodness factor
μ = dynamic viscosity
ϑ = time
Θ = period
ρ = density

Subscripts

b = bulk
Nu = associated with the Nusselt number
w = wall
0 = associated with the smooth duct

International Journal of Numerical Methods for Heat & Fluid Flow, Vol. 12 No. 5, 2002, pp. 610-628.

DOI 10.1108/09615530210434313

Introduction

Heat transfer enhancement can be achieved by employing surface modifications that generate secondary flows and/or destabilise the main flow. The resulting vortices move the fluid from the walls to the centre, reducing the thickness of the boundary layers. This is the case, for example, with angled and transverse ribs utilised to augment heat transfer in channels. Technical applications include internal cooling of the first rows of guiding vanes and blades in gas turbines. In the literature many data are available for channels with transverse ribs, e.g. see (Webb *et al.*, 1971; Webb and Ramadhyani *et al.*, 1985), Berner *et al.* (1984), Kelkar and Patankar (1987), Cheung and Huang (1991), Lopez *et al.* (1996) and Müller and Fiebig (1997). On the contrary, the effect of angled ribs has been taken into account only recently, e.g. see (Kukreja *et al.*, 1993; Kukreja and Lau, 1998), Sundén (1999) and Nonino and Comini (2000).

In this paper, the three-dimensional laminar forced convective heat transfer in ribbed square channels is investigated. The rib height is assumed to be 1/10 of the channel height. Numerical simulations are carried out employing a finite element procedure based on the equal order projection algorithm illustrated by (Nonino and Comini, 1997; Nonino *et al.*, 1997). This procedure shares many features with the well-known SIMPLE/SIMPLER algorithms, described by Patankar (1980). At each time step, a tentative pressure field is estimated first from a pressure-Poisson equation obtained by enforcing continuity on the pseudovelocities, i.e. on the velocities that would prevail in the absence of the pressure field. Then, the momentum equations are solved in sequence for velocity components, and continuity is enforced again to find corrections that modify both the velocity field and the estimated pressure field. Finally, the energy equation is solved before moving to the next step. In the finite element solution, equal order interpolation can be utilized for velocity and pressure variables because pressure equations are derived from continuous, rather than discretized, approximations.

In ribbed channels, transverse and angled ribs are placed on one wall or on two facing walls, to form a repetitive geometry. In this way, after a short distance from the entrance, also the flow and the dimensionless thermal fields repeat themselves from module to module allowing the assumption of periodic, or anti-periodic, conditions at the inlet/outlet sections of the calculation cell. As pointed out by Nonino and Comini (1998), periodic conditions arise when the ribs are placed on one channel wall, while anti-periodic conditions arise when the ribs are placed on both walls. Prescribed temperature boundary conditions are assumed at all solid walls, including the ribs.

Pressure drop and heat transfer characteristics in the ribbed channels are compared for different angles ranging from 90° (transverse ribs) to 45°. In all the situations investigated, pressure losses are much higher than the ones corresponding to the smooth channel. On the contrary, at low Reynolds

numbers a significant improvement of average heat transfer rates can be obtained only for angled ribs in anti-periodic configurations. This improvement can be explained by the formation of two counter-rotating longitudinal vortices that move the fluid from the walls to the centre. In the periodic case with angled ribs, only one longitudinal vortex appears and no mixing occurs between near wall and centre flows. With transverse ribs, the vortices are also transversal and the mixing effect is not much effective, at least at low values of the Reynolds number. On the other hand, the situation changes at Reynolds numbers above a critical value that corresponds to the onset of the self-sustained oscillations preceding the transition to turbulence. In fact, when the flow and temperature fields become unsteady, a new convective heat transfer mechanism appears: the periodic washing of the upper and lower channel walls by travelling transverse vortices. These vortices move the fluid particles from near the walls to the core and downstream, significantly enhancing the energy transport.

Statement of the problem

The three-dimensional geometry considered is made up of the repetition of identical modules in a square channel. The bottom, or the bottom and the top walls of the channel are roughened with vertical ribs, as illustrated in Figures 1(a) and 1(b), respectively. The perfectly conductive ribs are at the same temperature of the wall, have a negligible thickness and are characterised by a height equal to 1/10 of the channel height H. The width W of the channel and the length L of a module are both equal to H. The rib configurations of interest

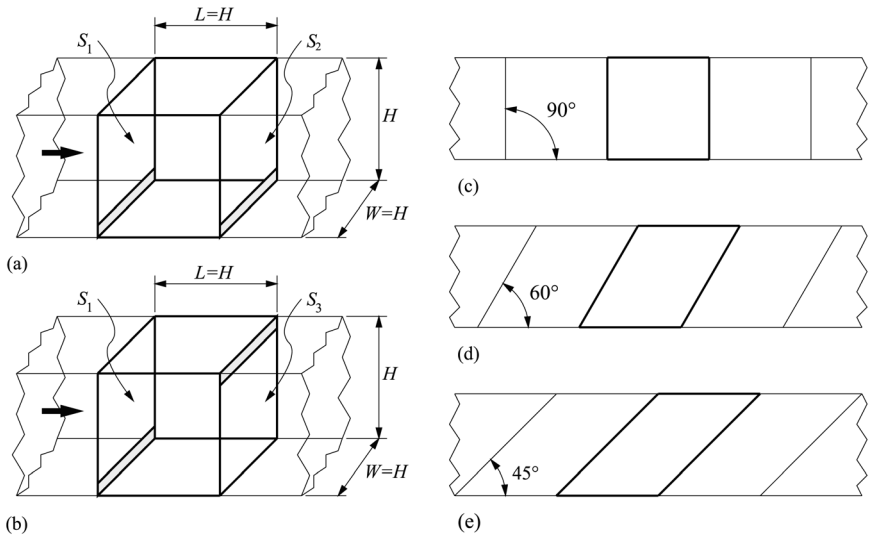

Figure 1.
Ribbed square channels: (a) periodic boundaries with one-sided ribs, (b) anti-periodic boundaries with staggered ribs, (c) transverse, 90° angled ribs, (d) 60° angled ribs and (e) 45° angled ribs

are transverse ribs (90°), 60° and 45° angled ribs, as shown in Figure 1(c,d,e), respectively.

After a short distance from the entrance of the channel, the flow and thermal fields repeat themselves from module to module, attaining a fully developed character. The repetitive flow and thermal fields allow the limitation of the analysis to a single module. In fact, it can be easily inferred that the distributions of velocity components and dimensionless temperatures at periodic boundaries, such as S_1 and S_2 in Figure 1(a), can be expressed as a periodic function. When the ribs are staggered, it is still possible to reduce the computational domain to a single module enclosed by anti-periodic boundaries, such as S_1 and S_3 in Figure 1(b). In this case, however, the relationships between velocity components and temperatures distributions on S_1 and S_3 must be expressed as anti-periodic functions.

The flow and temperature fields

Assuming the thermophysical properties of the fluid to be constant and the flow to be laminar, the governing equations are the standard Navier-Stokes, continuity and energy equations. They can be written in as

$$\rho\frac{\partial \mathbf{v}}{\partial \vartheta} + \rho\mathbf{v}\cdot\nabla\mathbf{v} = \mu\nabla^2\mathbf{v} - \nabla p \tag{1}$$

$$\nabla\cdot\mathbf{v} = 0 \tag{2}$$

In the above equations, $\mathbf{v}$ is the velocity vector, ϑ is the time, ρ is the density, μ is the dynamic viscosity, and p is the deviation from the hydrostatic pressure. In the absence of volumetric heating and neglecting the effects of viscous dissipation, the energy equation can be written as

$$\rho c\frac{\partial t}{\partial \vartheta} + \rho c\mathbf{v}\cdot\nabla t = k\nabla^2 t \tag{3}$$

where c is the specific heat and k is the thermal conductivity.

In a periodic fully developed flow, the pressure p can be expressed as the sum of a linear term, accounting for the overall pressure gradient, and a residual term that behaves in a periodic manner. Thus, with reference to the situation illustrated in Figure 1, we have

$$p = -\alpha x + \tilde{p} \tag{4}$$

where α is a constant representing the overall pressure gradient in the flow direction x and $\tilde{p}$ is the periodic component. The symmetric periodicity of $\tilde{p}$ between the boundaries S_1 and S_2 leads to the condition

$$\tilde{p}(L, y, z) = \tilde{p}(0, y, z) \tag{5}$$

while the antisymmetric periodicity between the boundaries S_1 and S_3 yields the condition

$$\tilde{p}(L, y, H - z) = \tilde{p}(0, y, z) \tag{6}$$

where z is the distance from the bottom boundary measured in the vertical direction and H is the height of the channel.

Appropriate conditions must be specified at wall and at periodic boundaries. At wall boundaries, the no-slip condition holds good

$$u = v = \mathrm{w} = 0 \tag{7}$$

The symmetric periodicity between the boundaries S_1 and S_2 leads to the conditions

$$\begin{aligned} u(L, y, z) &= u(0, y, z) \\ v(L, y, z) &= v(0, y, z) \\ \mathrm{w}(L, y, z) &= \mathrm{w}(0, y, z) \end{aligned} \tag{8}$$

while the anti-symmetric periodicity between the boundaries S_1 and S_3 leads to the conditions

$$\begin{aligned} u(L, y, H - z) &= u(0, y, z) \\ v(L, y, H - z) &= v(0, y, z) \\ \mathrm{w}(L, y, H - z) &= \mathrm{w}(0, y, z) \end{aligned} \tag{9}$$

Conditions (8) and (9) do not involve the specification of any inflow velocities. Thus the pressure gradient α must be adjusted iteratively, as described by Nonino and Comini (1998), to obtain the desired value of the average velocity

$$\bar{u} = \frac{1}{S} \int_S u \mathrm{d}S \tag{10}$$

on the cross-section S.

The behaviour of the flow is determined by the Reynolds number

$$\mathrm{Re} = \frac{\rho \bar{u} H}{\mu} = \frac{\dot{m}}{\mu H} \tag{11}$$

and is be characterized by the friction factor

$$f = \frac{\alpha H}{2 \rho \bar{u}^2} \tag{12}$$

which is directly related to the overall pressure gradient.

The wall boundary condition utilized for temperature is

$$t = t_w = \text{const} \tag{13}$$

In such a case, the distribution of the dimensionless temperature

$$T = \frac{t - t_w}{t_b - t_w} \tag{14}$$

identically repeats itself from module to module, as pointed out by Kelkar and Patankar (1987), and Nonino and Comini (1998).

In the above equation, t_b is the bulk temperature defined as

$$t_b = \frac{\int_{S'} |\mathbf{v}\cdot\mathbf{n}| t \mathrm{d}S}{\int_{S'} |\mathbf{v}\cdot\mathbf{n}| \mathrm{d}S} \tag{15}$$

where S' is the area of the surface parallel to the inflow/outflow boundaries, and $\mathbf{n}$ is the unit vector normal to the surface. Thus, the symmetric periodicity of T between the boundaries S_1 and S_2 leads to the condition

$$\frac{t(L,y,z) - t_w}{t_b(L) - t_w} = \frac{t(0,y,z) - t_w}{t_b(0) - t_w} \tag{16}$$

which can be written in the form

$$t(L,y,z) = \left[1 + \frac{t_b(L) - t_b(0)}{t_b(0) - t_w}\right] t(0,y,z) - \frac{t_b(L) - t_b(0)}{t_b(0) - t_w} t_w \tag{17}$$

Similarly, the antisymmetric periodicity between the boundaries S_1 and S_3 leads to the condition

$$\frac{t(L,y,H-z) - t_w}{t_b(L) - t_w} = \frac{t(0,y,z) - t_w}{t_b(0) - t_w} \tag{18}$$

which can be written in the form

$$t(L,H-y,z) = \left[1 + \frac{t_b(L) - t_b(0)}{t_b(0) - t_w}\right] t(0,y,z) - \frac{t_b(L) - t_b(0)}{t_b(0) - t_w} t_w \tag{19}$$

Equations (17) and (19) contain two unknown quantities: the bulk temperature at inflow $t_b(0)$ and the difference between the bulk temperatures at outflow and inflow. However, in the solution process we can first impose the value of the difference in the bulk temperatures, and then we can iterate until convergence is reached for a value of $t_b(0)$ which verifies the periodicity condition.

The overall Nusselt number is defined as

$$\mathrm{Nu} = \frac{hH}{k} \tag{20}$$

where

$$h = \frac{q}{S_0\ \overline{\Delta t}} \tag{21}$$

is the overall heat transfer coefficient, S_0 is the heat transfer surface pertaining to the corresponding module of a smooth channel, q is the total heat flow rate and

$$\overline{\Delta t} = \Delta t_{ml} = \frac{[t_\mathrm{w} - t_\mathrm{b}(L)] - [t_\mathrm{w} - t_\mathrm{b}(0)]}{\ln\{[t_\mathrm{w} - t_\mathrm{b}(L)]/[t_\mathrm{w} - t_\mathrm{b}(0)]\}} \tag{22}$$

is the logarithmic mean temperature difference.

Numerical solution

In the procedure adopted, the momentum, continuity and energy equations are solved by the equal-order, velocity-pressure algorithm for incompressible thermal flows described by Nonino and Comini (1997). As already pointed out, the velocity-pressure coupling is handled by a methodology, which shares many features with the SIMPLE/SIMPLER algorithm illustrated by Patankar (1980). At each new time step $(n+1)$ the pseudovelocity field (u, v, w), which can be obtained by neglecting the pressure gradients in the momentum equations, is computed from the velocity field (u^n, v^n, w^n), which prevails at the end of the old time step (n). Then, by enforcing continuity on the pseudo-velocity field, a tentative pressure p^* is estimated, and the momentum equations are solved for the tentative velocity field (u^*, v^*, w^*). Afterwards, continuity is enforced again to find pressure corrections p' which yield $p^{n+1} = p^* + p'$. Pressure corrections are also used to find the velocity corrections (u', v', w') that [project] (u^*, v^*, w^*) onto the divergence-free space $(u^{n+1} = u^* + u',\ v^{n+1} = v^* + v',\ w^{n+1} = w^* + w')$. Once the velocity field $(u^{n+1}, v^{n+1}, w^{n+1})$ has been found, the energy equation can be solved before moving to the next step.

As illustrated by Comini *et al.* (1994), the momentum and energy equations are particular versions of the transport equation for a generic dependent variable a. This equation can be written in the time-discretized form

$$\gamma\frac{a^{n+1} - a^n}{\Delta\vartheta} + \gamma\mathbf{v}^n\cdot[\tau\nabla a^{n+1} + (1-\tau)\nabla a^n]$$
$$= \Gamma[\tau_\Gamma\nabla^2 a^{n+1} + (1-\tau_\Gamma)\nabla^2 a^n] + \dot{s} \tag{23}$$

The properties γ and Γ, and the volumetric source rate $\dot{s}$ can be easily identified by inspection of the appropriate original equations. The weighting factors τ_v

and τ_Γ, both in the range from 0 to 1, allow the selection of different time-integration schemes. Finally, it must be pointed out that the pressure equation and the pressure correction equation are particular versions of the Poisson equation, which can be obtained from equation (23) by assuming $\gamma = 0$ and $\tau_\Gamma = \Gamma = 1$.

The space discretization of the general transport equation is based on the Galerkin method. In fact, for each node i we obtain an integral form by weighting and integrating equation (23) over the computational domain. The application of Green's theorem to the diffusion terms at the right hand side of equation (23) yields the weak forms, and allows the introduction of Neumann boundary conditions.

As usual, the unknown functions are approximated throughout the solution domain by the expansions

$$a = \sum N_j a_j = \mathbf{Na} \tag{23}$$

where a_j stand for the nodal values, while N_j are interpolating functions. In the Bubnov-Galerkin method utilized here, N_j coincide with the weighting functions employed in the weak forms. Therefore, no upwinding techniques are employed.

Substituting equation (24) into the appropriate weak forms, we arrive at systems of space discretized equations that can be written as

$$\mathbf{Ha} = \mathbf{g} \tag{24}$$

where $\mathbf{a}$ is the vector of nodal values, $\mathbf{H}$ is the effective stiffness matrix, accounting for all homogeneous contributions, and $\mathbf{g}$ is the effective load vector, accounting for all nonhomogeneous contributions. Finally, the boundary conditions of the first kind at the walls are implemented in the usual way, e.g. see Comini *et al.* (1994). The periodic boundary conditions are introduced as illustrated in detail by Nonino and Comini (1998). In particular it must be noticed that, with reference to the corresponding points on the inflow (i) and outflow (o) boundaries, all the periodic boundary conditions above illustrated can be expressed in the general form

$$a_o = Ba_i + D \tag{25}$$

where the values of B and D can be easily inferred from the physical boundary conditions

- (5) and (6) for the periodic components of pressure;
- (8) and (9) for the velocity components;
- (17) and (19) for the fluid temperature.

Accordingly, the matrix **H** and the right hand side vector **g** in equation (24) are modified to take into account equation (25).

At each time step the systems of linear equations, arising from the discretization process, were solved by means of iterative algorithms. The conjugate gradient squared (CGS) method has been used to solve the discretized momentum and energy equations, while the conjugate residual (CR) method has been used to solve the symmetric systems obtained from the discretization of the Poisson equations. In both cases, preconditioned matrices have been obtained from an incomplete LU decomposition (ILU).

Results

The calculations presented in the following concern steady- and unsteady-state solutions that have been obtained from pseudo-transient, or transient, simulations, respectively. In the simulations we used structured grids of eight-node trilinear (brick) elements, with finer grid spacings near the walls and near the inflow and outflow sections. Grid independence was established on the basis of preliminary calculations in which the distance between grid points was progressively reduced by 30 per cent from one simulation to another. When a further decrease led to a change in the average Nusselt numbers smaller that 1 per cent, the results were considered to be grid-independent. In the final simulations we used a mesh consisting of $31 \times 31 \times 33 = 31713$ nodal points and 28800 elements. Time-step independence was also established on the basis of preliminary calculations in which the dimensionless time step $\bar{u}\Delta\vartheta/L$ was progressively reduced by 30 per cent from one simulation to another. When a further decrease led to a change in the average Nusselt numbers smaller that 1 per cent, the results were considered to be independent on the time step. In the final simulations we used a dimensionless time step equal to 0.01 with a Crank-Nicolson scheme for the transient solutions, and a dimensionless values of the time step equal to 0.02 with a fully implicit scheme for the steady-state solutions.

The reliability of the procedure described in the previous section had already been demonstrated by Nonino and Croce (1997), and Nonino and Comini (1998). However, the accuracy has been assessed once again imposing the symmetric periodicity conditions on a portion of a smooth square channel. In this way we obtained $\mathrm{Nu}_0 = 2.972$ and $(f\mathrm{Re})_0 = 14.25$ for the fully developed flow and thermal fields, respectively. As expected, these results are independent of the Reynolds and Prandtl number and agree to the 3rd figure with the analytical solutions $\mathrm{Nu}_0 = 2.976$ and $(f\mathrm{Re})_0 = 14.227$, reported by Shah and London (1978, p. 200).

The calculations for all rib-roughened channels have been carried out for a Prandtl number $\mathrm{Pr} = 0.7$, and a range of Reynolds numbers from $\mathrm{Re} = 100$ to upper values in the regime which precedes the transition to turbulence. Above a critical value of the Reynolds number Re_{cr}, the flow character changes first

from stationary to time-periodic, and then to nearly chaotic. In time-periodic and nearly chaotic situations, overall parameters were further averaged over a period or a suitable time interval, respectively, yielding single representative values. This way we obtained

$$\langle \varphi \rangle = \frac{1}{\Theta} \int_{\vartheta}^{\vartheta+\Theta} \phi(\vartheta) \mathrm{d}\vartheta \tag{26}$$

where $\varphi = f$, Nu or $\mathbf{v}$. To lighten the notation, the symbol $\langle\rangle$ has been omitted in the following, except when referred to the time averaged velocity vectors.

As pointed out in the Introduction, the aim of the paper is to investigate the influence of the rib geometry, and the effect of self-sustained flow oscillations that arise for $\mathrm{Re} > \mathrm{Re}_{cr}$ before the flow becomes turbulent. These investigations are illustrated below.

Influence of rib geometries

The influence of rib geometries is best established with reference to stationary flows in the sub-critical range. At $\mathrm{Re} = 300$, we have such flows in all the rib-roughened channels considered. The corresponding fields are illustrated in Figure 2 by plotting trajectories and velocity vectors, and in Figure 3 by plotting pressure contours on two adjacent walls. As can be seen from Figure 2, the staggered angled ribs induce two longitudinal counter-rotating vortices, which move the fluid from the walls to the centre of the channels. On the contrary, the non-staggered angled ribs induce only one longitudinal vortex and, practically, no mixing between near-wall and centre flows. Finally, transverse ribs induce transverse vortices which are not much effective as mixing promoters. Thus it can be expected that only the staggered angled ribs have a beneficial effect on the heat transfer rate, even if all rib configurations increase pressure losses.

Influence of flow oscillations

The influence of flow oscillations can be best established with reference to the time dependent velocity fields that arise above the critical value of the Reynolds number. Let us consider, for example, the vertical mid-plane $y/W = 0.5$ in a square channel with staggered, 45° angled ribs. At $\mathrm{Re} = 675$ (a higher than critical value) the flow is time-periodic, and the projection of the differences $\mathbf{v} - \langle \mathbf{v} \rangle$ between instantaneous and time-averaged velocity vectors behave as shown in Figure 4. It appears that the upper and lower channel walls are washed by transverse vortices that detach periodically from the ribs and move downstream. This process transports fluid particles from the walls to the core and downstream, thus enhancing the energy transfer. Similar results would have been obtained for all the rib geometries, above the critical value of the Reynolds number.

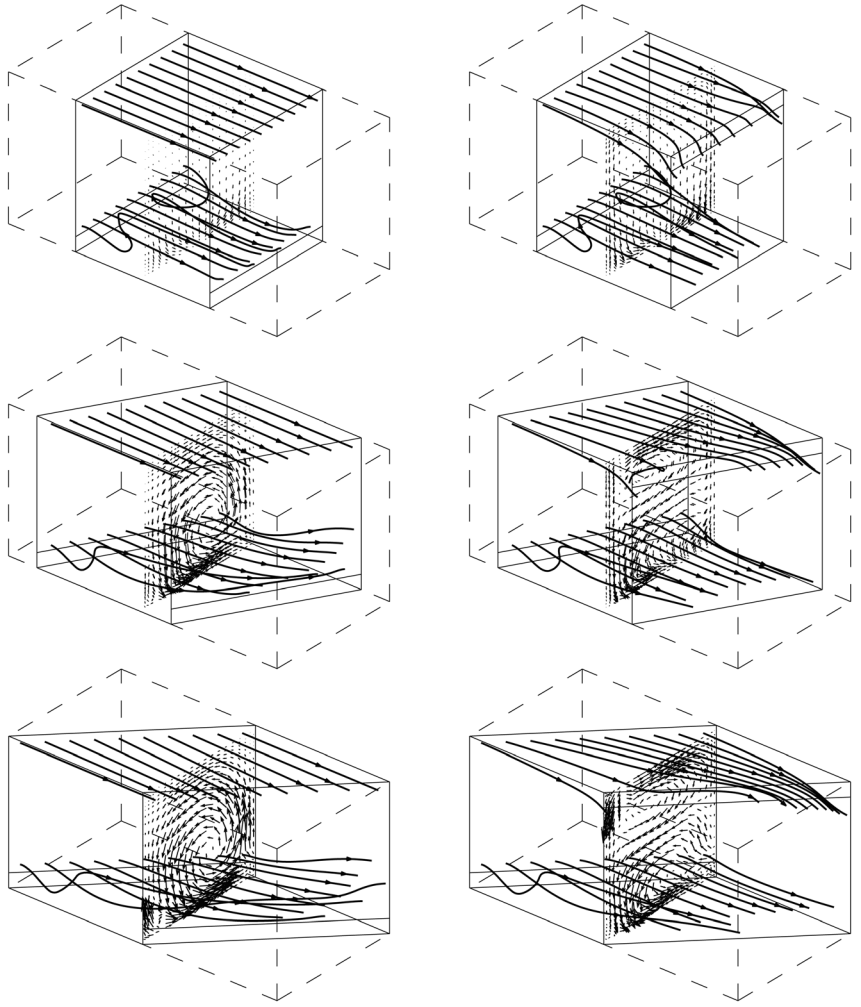

Figure 2.
Trajectories and transverse velocity vectors at Re = 300 in square channels with 90°, 60° and 45° angled ribs (one-sided ribs on the left; staggered ribs on the right)

The value of the critical Reynolds number depends on the geometrical configuration. Its direct calculation is an almost impossible task because the transients become longer and longer as one approaches the critical point, and the amplitude of the oscillations tends to zero. The results of Table I are slightly above the critical values and have been found by a trial-and-error procedure.

Transition to turbulence

When the Reynolds number increases above the critical value, the flow starts a transition towards the turbulent regime. In the literature, two routes from the

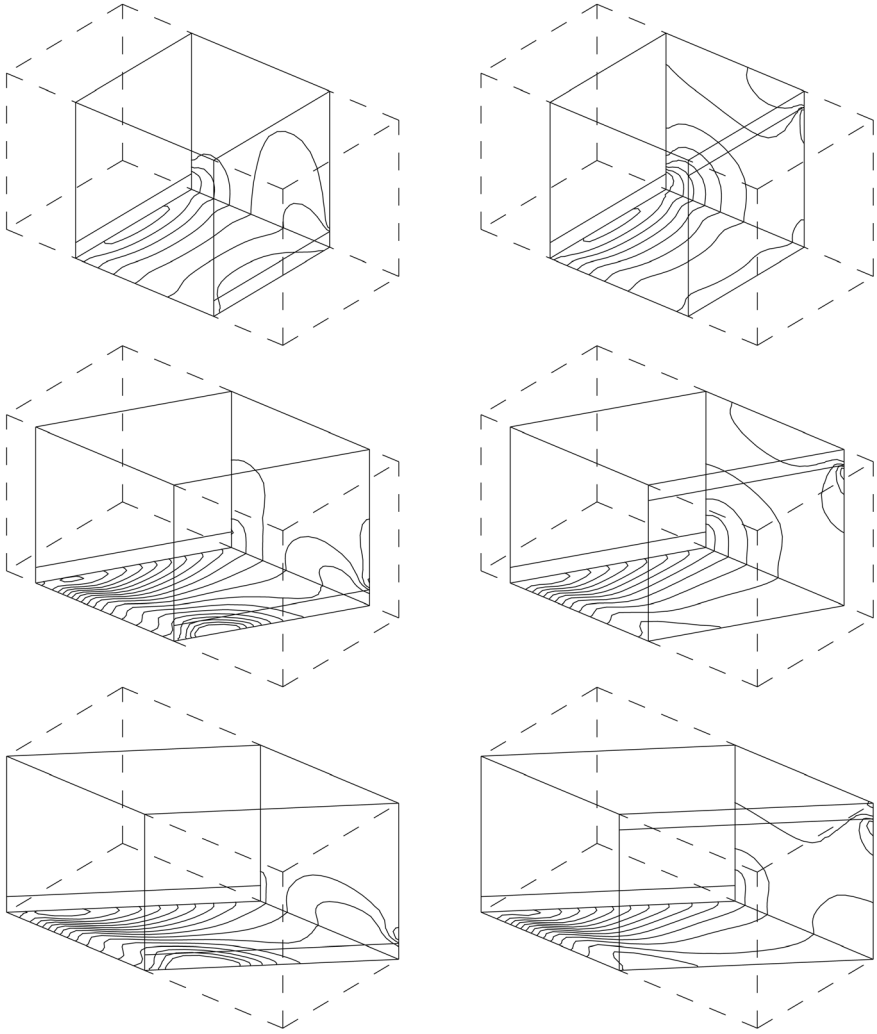

Figure 3.
Pressure contours at Re = 300 on two walls of square channels with 90°, 60° and 45° angled ribs (one-sided ribs on the left; staggered ribs on the right)

time-periodic to the turbulent regime have been classified and investigated extensively. The route described by Ruelle and Takens (1971) involves two main bifurcations. The first bifurcation leads to a semi-periodic regime characterized by the appearance of a second dominant frequency, incommensurate with respect to the existing one. When a further bifurcation brings about a third incommensurate frequency, the flow becomes turbulent. The route described by Feigenbaun (1978) involves a series of successive frequency halving bifurcations or, according to Libchaber and Maurer (1981), alternative series of one-third or, even, one-fifth frequency reductions. In the

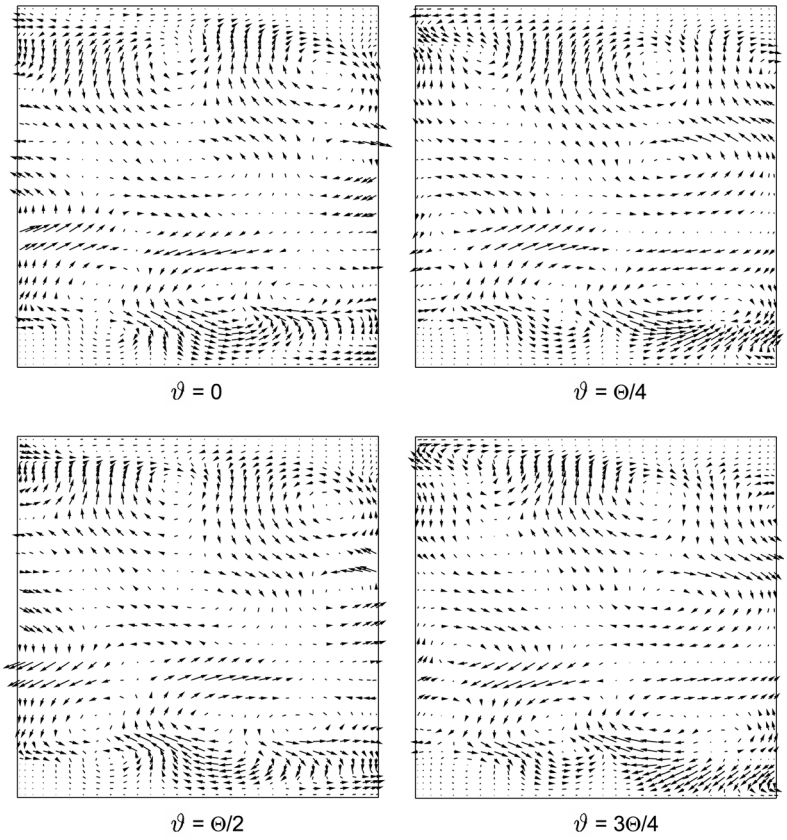

Figure 4.
Differences between instantaneous and time-averaged velocity vectors in the vertical mid-plane $y/W = 0.5$ of a 45° angled square channel, at $\mathrm{Re} = 675$ and $\Theta/4$ intervals

Fourier space, these inverse cascades yield first a broadening of the spectrum and, finally, a transition to chaos.

In the flows investigated here, the Feigenbaun scenario seems to prevail, even if it must be pointed out that, sometimes, flow transitions cannot be easily detected. In transverse ribbed channels, for example, successive bifurcations arise at quite closely spaced Reynolds numbers. On the contrary, in channels with angled ribs transitions to turbulence take place in a fairly large interval of

Table I.
Values of the critical Reynolds number in rib-roughened, square channels

Rib angle	One-sided ribs	Staggered ribs
90°	> 1100	> 700
60°	860	615
45°	1080	675

Reynolds numbers. For the sake of brevity, in the following we will consider only the square channel with 45° angled, staggered ribs. The behaviour of the flow in this channel is illustrated in Figure 5. In this figure we consider first the time variations of the space-averaged Nusselt number, then the corresponding power density spectra and, finally, the (u, w) phase trajectories at a reference point in the centre of the inflow section. At $\mathrm{Re} = 675$, both the Nu vs. ϑ representation and the phase diagram (a closed curve) indicate that the time behaviour is periodic. Correspondingly, the fast Fourier transform shows a dominant frequency, whose dimensionless value is $\mathrm{St} \cong 1.49$ when expressed in terms of the Strouhal number

$$\mathrm{St} = \frac{H}{\Theta \bar{u}} \tag{27}$$

At $\mathrm{Re} = 700$ and $\mathrm{Re} = 725$ the flow is quasi-periodic, as can be inferred from the Nu vs. ϑ representation. Correspondingly the phase diagrams become "almost closed" curves, and the fast Fourier transforms show much broader spectra with respect to the $\mathrm{Re} = 675$ case. The ratio between the dominant frequencies is about one fifth, both in the $\mathrm{Re} = 700$ vs. $\mathrm{Re} = 675$ case and in the $\mathrm{Re} = 725$ vs. $\mathrm{Re} = 675$ case. A further increase in the Reynolds number to $\mathrm{Re} = 775$ leads to a quasi-chaotic behaviour, as can be inferred from the Nu vs. ϑ representation. Correspondingly, the phase diagram does not exhibit any repetitive pattern, and the Fourier transform shows a quite distributed spectrum over a broad frequency range.

Quantitative comparisons

The momentum and heat transfer characteristics of ribbed channels can be described in terms of apparent friction factors multiplied by the Reynolds number (f Re parameter) and overall Nusselt numbers (Nu). The f Re and Nu values pertaining to the ribbed channels are divided by the corresponding values pertaining to the fully developed flow and thermal fields in a smooth straight channel. These quantitative findings are reported in Figure 6 for different Reynolds numbers up to the critical value.

In boundary layer flows, the momentum and heat transfer characteristics are related by the Chilton-Colburn analogy, which can be written in the form

$$\varepsilon = \frac{j}{f} = \frac{\overline{\mathrm{Nu}}}{\mathrm{Re}\ \mathrm{Pr}^{1/3}} \frac{1}{f} = \mathrm{const} \tag{28}$$

where ε can be interpreted as a goodness factor. This analogy is strictly valid for boundary layer flows over a flat plate. However, by adjusting the value of the constant, it can be applied with good results to any non-recirculating flow. For example, in the case of $\mathrm{Pr} = 0.7$ and fully developed laminar flow and thermal fields in a straight square channel, we obtain

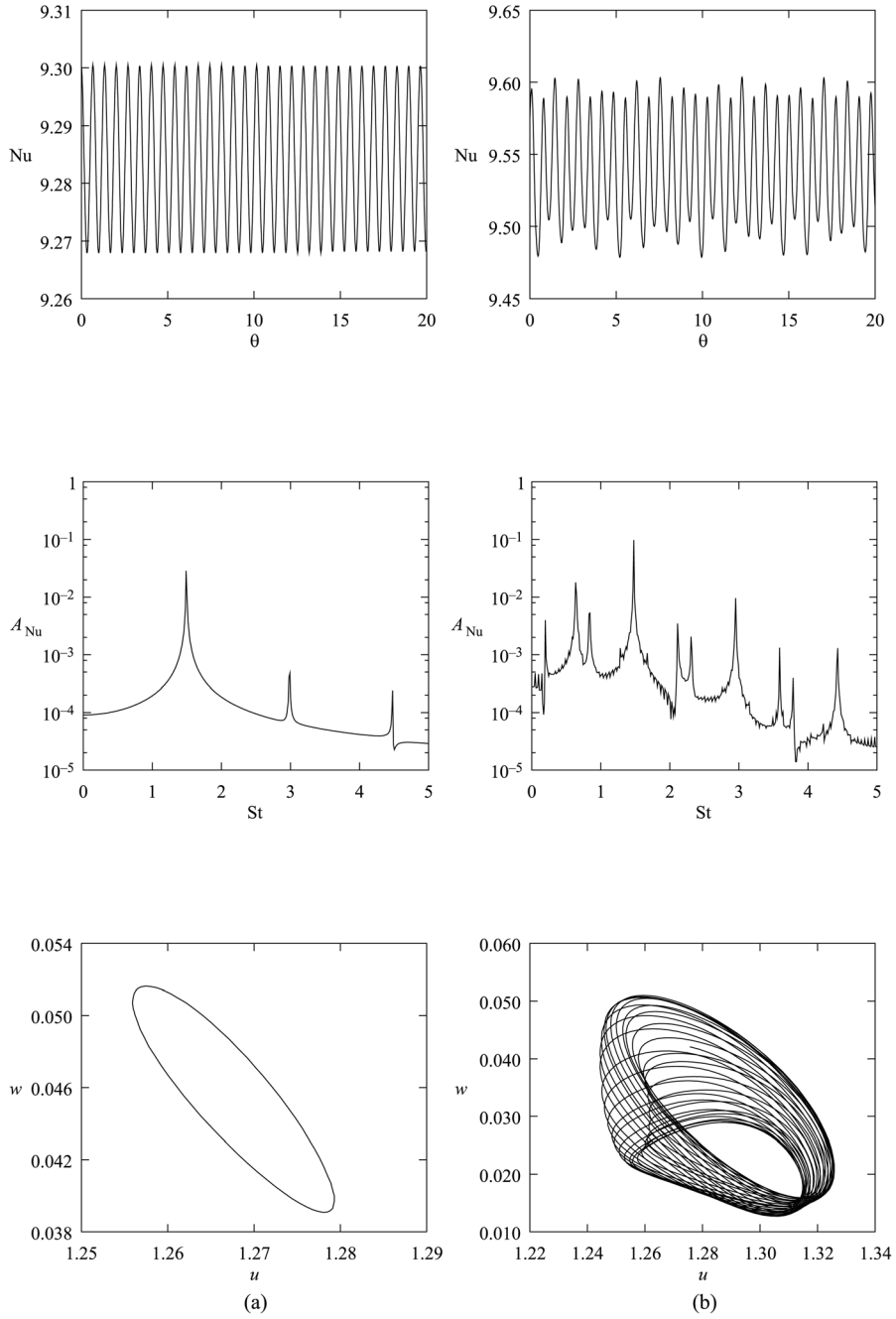

Figure 5.
Square channel with staggered 45° angled ribs: time behaviour of the space-averaged Nusselt number (top), corresponding power density spectra (centre) and (u, w) phase trajectories (bottom), at (a) Re = 675, (b) Re = 700, (c) Re = 725 and (d) Re = 775.

(*Continued*)

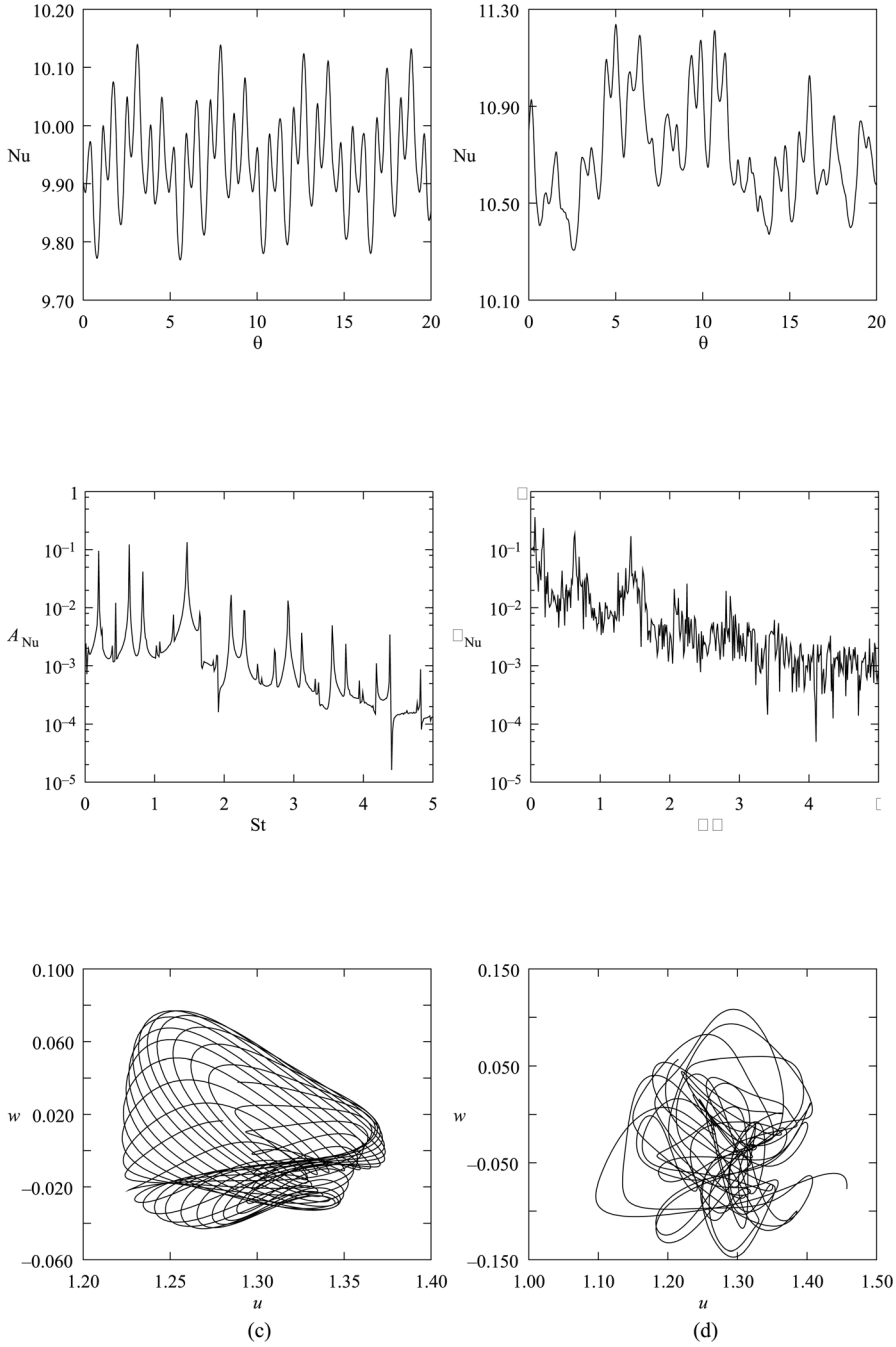
10.20
10.10
10.00
9.90
9.80
9.70
Nu
0
5
10
15
20
θ
11.30
10.90
10.50
10.10
Nu
0
5
10
15
20
θ
1
10−1
10−2
10−3
10−4
10−5
ANu
0
1
2
3
4
5
St
10−1
10−2
10−3
10−4
10−5
Nu
0
1
2
3
4
0.100
0.060
0.020
−0.020
−0.060
w
1.20
1.25
1.30
1.35
1.40
u
(c)
0.150
0.050
−0.050
−0.150
w
1.00
1.10
1.20
1.30
1.40
1.50
u
(d)

Figure 5.

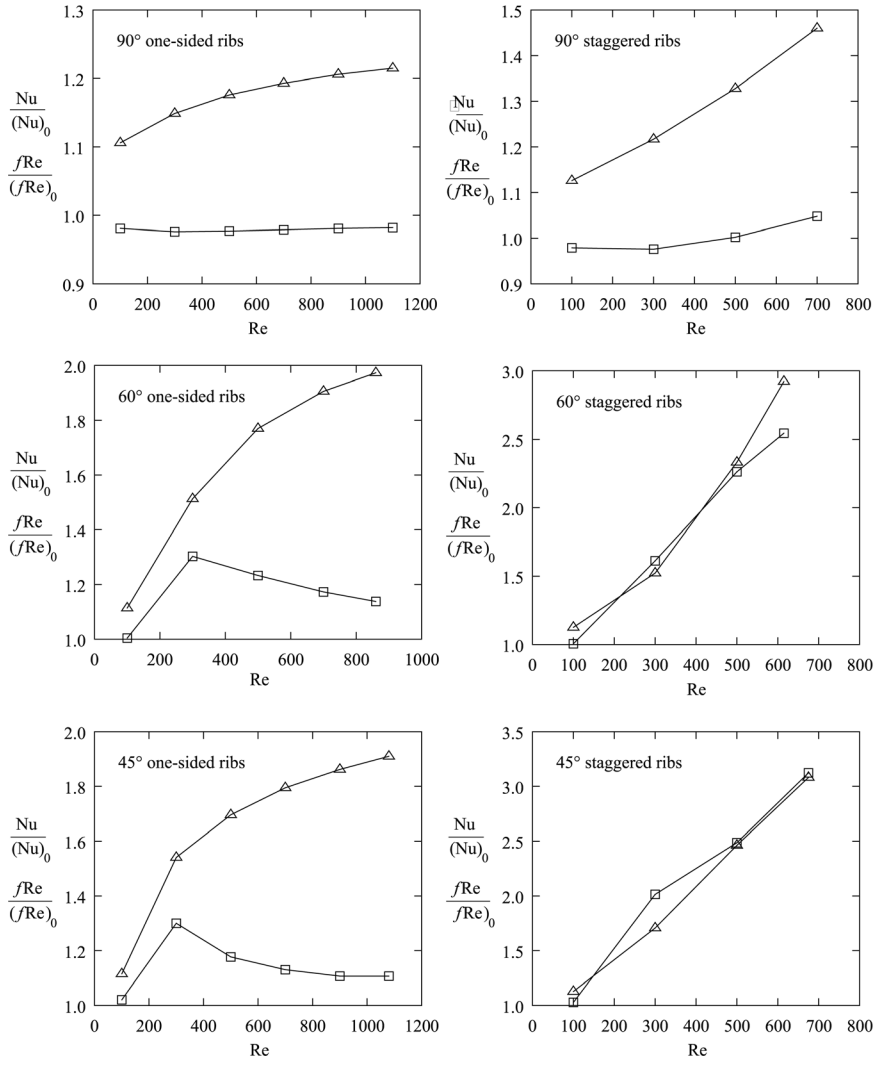

Figure 6.
Apparent friction factors (triangles) and overall Nusselt numbers (squares) in ribbed square channels, normalized with corresponding values for smooth square ducts

$$\varepsilon_0 = \left(\frac{j}{f}\right)_0 = \frac{\overline{\mathrm{Nu}}_0}{(f\ \mathrm{Re})_0\ \mathrm{Pr}^{1/3}} = 0.236 \tag{29}$$

In recirculating flows, such as the ones occurring in ribbed channels, the Chilton-Colburn analogy cannot be expected to hold good. However, the ratio $\varepsilon/\varepsilon_0$ can still be used as a goodness factor in performance comparisons such as the ones reported in Figure 7.

These comparisons are in good agreement with previous considerations. In fact, the 45° angled, staggered ribs perfom better than the other staggered ribs.

Similarly, the staggered ribs perform better than the non-staggered ones.

Conclusions

Pressure drop and heat transfer characteristics in rib-roughened, square channels have been investigated for different values of the Reynolds number. In all the situations considered, the fRe parameter of the ribbed channels is much higher than the one corresponding to the smooth channel.

On the contrary, a significant improvement of the average Nusselt number can be obtained only for angled ribs in anti-periodic configurations and relatively high values of the Reynolds number. This improvement can be attributed to the formation of longitudinal vortices that mix near wall and centre flows. The non-staggered, angled ribs are not effective since they induce only one longitudinal vortex and, practically, no mixing between near-wall and centre flows.

Finally, transverse ribs induce transverse vortices that do not promote any mixing, at least for Reynolds number below the critical value corresponding to the onset of self-sustained oscillations. When the flow and temperature fields become unsteady, a new convective heat transfer mechanism appears: the periodic washing of the upper and lower channel walls by travelling transverse vortices. This process transports fluid particles from the walls to the core and downstream, enhancing the energy transfer.

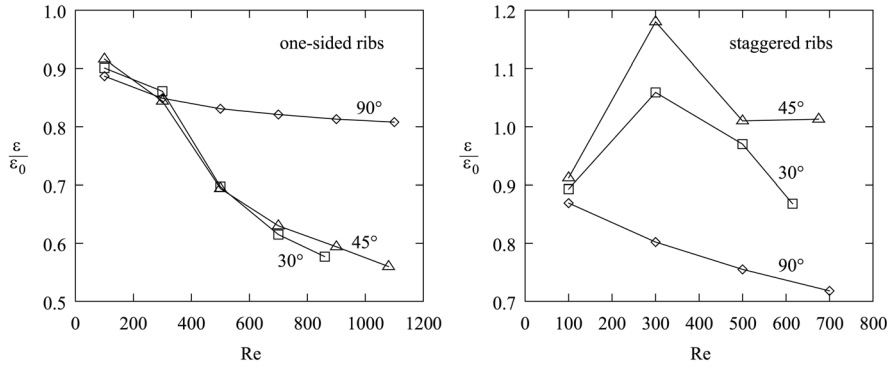

Figure 7.
Goodness factors in ribbed square channels, normalized with corresponding values for smooth square ducts

References

Berner, C., Durst, F. and McEligot, D.M. (1984), "Flow around baffles", *ASME J. Heat Transfer*, Vol. 106, pp. 743-9.

Cheung, C.H. and Huang, W.H. (1991), "Numerical prediction for laminar forced convection in parallel-plate channels with transverse fin arrays", *Int. J. Heat Mass Transfer*, Vol. 34, pp. 2739-49.

Comini, G., Del Giudice, S. and Nonino, C. (1994), *Finite Element Analysis in Heat Transfer: Basic Formulation and Linear Problems*, Taylor & Francis, Washington, DC.

Feigenbaum, M.J. (1978), "Quantitative universality for a class of nonlinear transformations", *Journal of Statistical Physics*, Vol. 19, pp. 24-52.

Kelkar, K.M. and Patankar, S.V. (1987), "Numerical prediction of flow and heat transfer in a parallel plate with staggered fins", *ASME J. Heat Transfer*, Vol. 109, pp. 25-30.

Kukreja, R.T. and Lau, S.C. (1998), "Distribution of local heat transfer coefficient on surfaces with solid and perforated ribs", *Enhanced Heat Transfer*, Vol. 5, pp. 9-21.

Kukreja, R.T., Lau, S.C. and McMillin, R.D. (1993), "Local heat/mass transfer distribution in a square channel with full and V-shaped ribs", *Int. J. Heat Mass Transfer*, Vol. 36, pp. 2013-20.

Libchaber, A. and Maurer, J. (1981), "A Rayleigh Bénard experiment: helium in a small box", in, *Nonlinear Phenomena at Phase Transitions and Instabilities*, Riste, T., (Eds) Plenum Press, New York pp. 259-86.

Lopez, J.R., Anad, N.K. and Fletcher, L.S. (1996), "Heat transfer in a three-dimensional channel with baffles", *Numerical Heat Transfer, Part A*, Vol. 30, pp. 189-205.

Müller, U. and Fiebig, M. (1997), "Instantaneous and time averaged 3d flow and temperature structure in 2d ribbed channels", in, *Advanced Concepts and Techniques in Thermal Modelling*, Henriette, J., Lybaert, P., El Hayek, M., (Eds) Elsevier, Paris pp. 223-30.

Nonino, C. and Comini, G. (1997), "An equal order pressure-velocity algorithm for incompressible thermal flows – Part 1: formulation", *Numer. Heat Transfer Part B*, Vol. 32, pp. 1-15.

Nonino, C. and Croce, G. (1997), "An equal order pressure-velocity algorithm for incompressible thermal flows – Part 2: validation", *Numer. Heat Transfer Part B*, Vol. 32, pp. 17-35.

Nonino, C. and Comini, G. (1998), "Finite-element analysis of convection problems in spatially periodic domains", *Numer. Heat Transfer Part B*, Vol. 34, pp. 361-78.

Nonino, C. and Comini, G. (2000), "Heat transfer in channels with transverse and angled ribs", in, *3rd European Thermal Sciences Conference*, Hahne, E.W.P., Heidemann, W., Spindler, K., (Eds) Edizioni ETS, Pisa pp. 319-24.

Nonino, C., Comini, G. and Croce, G. (1999), "Three-dimensional flows over backward facing steps", *International Journal of Numerical Methods for Heat & Fluid Flow*, Vol. 9, pp. 224-39.

Patankar, S.V. (1980), *Numerical Heat Transfer and Fluid Flow*, Hemisphere, Washington, D.C..

Ruelle, D. and Takens, F. (1971), "On the nature of turbulence", *Commun. Math. Phys.*, Vol. 20, pp. 167.

Sundén, B. (1999), "Enhancement of convective heat transfer in rib-roughened rectangular ducts", *Enhanced Heat Transfer*, Vol. 6, pp. 89-103.

Shah, R.K. and London, A.L. (1978), "Laminar Flow Forced Convection in Ducts", in, *Advances in Heat Transfer*, Supplement 1 Academic Press, New York 1978 pp.

Webb, B.W. and S. Ramadhyani, S. (1985), "Conjugate heat transfer in a channel with staggered ribs", *Int. J. Heat Mass Transfer*, Vol. 28, pp. 1679-87.

Webb, R.L., Eckert, E.R.G. and Goldstein, R. (1971), "Heat transfer and friction in tubes with repeated rib-roughness", *Int. J. Heat Mass Transfer*, Vol. 14, pp. 601-17.